THE CELL METHOD FOR CLASSICAL PLATE THEORY

by
Stephen V. Harren
http://www.harren.us

0. Contents

1. Governing Equations

Let u be the transverse displacement of the plate. Then, the rotation vector ϕ_i is

$$\varepsilon_{ij} = \begin{bmatrix} 0 & 1 \\ -1 & 0 \end{bmatrix} , \qquad \phi_i = \varepsilon_{ij} u_{,j} \quad \text{or} \quad \phi_x = u_{,y} , \qquad \phi_y = -u_{,x} , \tag{1.1}$$

where ε_{ij} is the two-dimensional alternating symbol, repeated indices are summed, and the comma denotes differentiation with respect to the (spatial) rectangular coordinates. The components of the curvature tensor κ_{ij} are

$$\kappa_{ij} = u_{,ij} \quad \text{or} \quad \kappa_{xx} = u_{,xx} , \qquad \kappa_{yy} = u_{,yy} , \qquad \kappa_{xy} = \kappa_{yx} = u_{,xy} . \tag{1.2}$$

Next, Hooke's Law for the plate is

$$D = \frac{Eh^3}{12(1-\nu^2)} , \qquad M_{xx} = -M_{yy} = D(1-\nu)\kappa_{xy} ,$$
$$M_{xy} = -D\left(\kappa_{xx} + \nu\kappa_{yy}\right) , \qquad M_{yx} = D\left(\nu\kappa_{xx} + \kappa_{yy}\right) , \tag{1.3}$$

where E is Young's modulus and ν is Poisson's ratio. In eqns. (1.3), M_{ij} are the components of the moment tensor, with M_{ij} being the moment vector acting in the j–direction on an internal face whose normal is the i–direction. Moment equilibrium is

$$V_x = M_{xy,x} + M_{yy,y} , \qquad V_y = -M_{xx,x} - M_{yx,y} , \tag{1.4}$$

where V_i are the components of the (transverse) shear vector (V_i is the transverse force per plate thickness on an internal face whose normal is in the i–direction). Notwithstanding, substitution of eqns. (1.2) and (1.3) into eqns. (1.4) gives

$$V_i = -Du_{,jji} \quad \text{or} \quad V_x = -D\left(u_{,xxx} + u_{,xyy}\right) , \qquad V_y = -D\left(u_{,xxy} + u_{,yyy}\right) . \tag{1.5}$$

Now, transverse equilibrium is

$$V_{i,i} + q = 0 \quad \text{or} \quad V_{x,x} + V_{y,y} + q = 0 , \tag{1.6}$$

where q is the transverse force per unit area acting on the plate. Finally, substituting eqns. (1.5) into (1.6) yields the governing equation of the plate

$$\nabla^4 u = u_{,iijj} = u_{,xxxx} + 2u_{,xxyy} + u_{,yyyy} = \frac{q}{D} , \tag{1.7}$$

where $\nabla^4 u$ is the bi-harmonic of u.

In polar coordinates, the components of the rotation vector are

$$\phi_r = \frac{1}{r} u_{,\theta} , \qquad \phi_\theta = -u_{,r} , \tag{1.8}$$

and the curvatures are

$$\kappa_{rr} = u_{,rr} , \qquad \kappa_{\theta\theta} = \frac{1}{r^2} u_{,\theta\theta} + \frac{1}{r} u_{,r} , \qquad \kappa_{r\theta} = \kappa_{\theta r} = \frac{1}{r} u_{,r\theta} - \frac{1}{r^2} u_{,\theta} . \tag{1.9}$$

In polar coordinates, Hooke's Law is the same as eqns. (1.3) with $x \to r$ and $y \to \theta$. In any case, the equations for the shear vector are

$$V_r = -D\left(u_{,rrr} + \frac{1}{r}u_{,rr} - \frac{1}{r^2}u_{,r} + \frac{1}{r^2}u_{,r\theta\theta} - \frac{2}{r^3}u_{,\theta\theta}\right),$$

$$V_\theta = -D\left(\frac{1}{r}u_{,rr\theta} + \frac{1}{r^2}u_{,r\theta} + \frac{1}{r^3}u_{,\theta\theta\theta}\right). \tag{1.10}$$

Finally, the bi-harmonic operator in eqn. (1.7) is

$$\nabla^4 u = u_{,rrrr} + \frac{2}{r}u_{,rrr} - \frac{1}{r^2}u_{,rr} + \frac{2}{r^2}u_{,rr\theta\theta} + \frac{1}{r^3}u_{,r} - \frac{2}{r^3}u_{,r\theta\theta} + \frac{4}{r^4}u_{,\theta\theta} + \frac{1}{r^4}u_{,\theta\theta\theta\theta}. \tag{1.11}$$

Finally, let **n** be the outward-pointing unit normal vector on the boundary of the domain, and **t** be the unit tangent vector along the boundary of the domain pointing in the counterclockwise sense. The moment vector $\boldsymbol{\mathcal{M}}$ acting on the boundary is $\boldsymbol{\mathcal{M}} = \mathbf{n}\cdot\mathbf{M}$ or $\mathcal{M}_j = n_i M_{ij}$. In the boundary nt–system, admissible boundary conditions are: prescribe either ϕ_t or $\mathcal{M}_t$ and either u or $\bar{V}_n$ at each point of the boundary, where $\bar{V}_n = V_n - \mathcal{M}_{n,t}$ is the Kirchhoff shear force.

2. Example in Rectangular Coordinates

Here, the solution to a simple problem in rectangular coordinates is presented, which problem will be solved numerically later with the cell method.

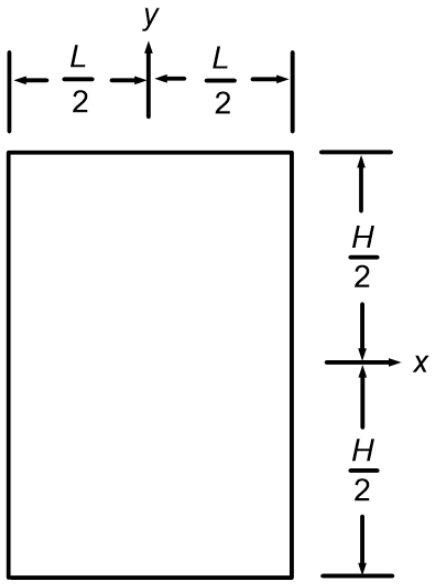

Figure 1. Domain of an L by H rectangular plate.

The domain of the rectangular plate under consideration is shown at left in Fig. 1. The plate is subject to the distributed load

$$q = -\frac{\pi^2 F}{4LH}\cos\left(\frac{\pi x}{L}\right)\cos\left(\frac{\pi y}{H}\right), \tag{2.1}$$

where $F > 0$ is the net downward force of the distribution, *i.e.,*

$$\int_A q\,\mathrm{d}A = -F. \tag{2.2}$$

Note that q is zero on the boundary and is maximum at the origin. On all four faces the boundary conditions are

$$u = 0, \qquad \mathcal{M}_t = 0, \tag{2.3}$$

which are the so-called "simply-supported" boundary conditions.

The governing eqn. (1.7) is, via eqn. (2.1),

$$u_{,xxxx} + 2u_{,xxyy} + u_{,yyyy} = -\frac{3\pi^2(1-\nu^2)F}{Eh^3LH}\cos\left(\frac{\pi x}{L}\right)\cos\left(\frac{\pi y}{H}\right), \tag{2.4}$$

which is solved with a displacement of the form

$$u = k\cos\left(\frac{\pi x}{L}\right)\cos\left(\frac{\pi y}{H}\right). \tag{2.5}$$

Substituting eqn. (2.5) into eqn. (2.4) gives that

$$k = -\frac{3(1-\nu^2)}{\pi^2 E h^3}\left[\frac{L^3H^3}{(L^2+H^2)^2}\right]F. \tag{2.6}$$

With eqns. (2.5) and (2.6) the problem is solved.

By differentiation of eqn. (2.5) by way of eqn. (1.1), the rotation vector is

$$\phi_x = \frac{3(1-\nu^2)}{\pi^2 E h^3}\left[\frac{L^3H^2}{(L^2+H^2)^2}\right]F\cos\left(\frac{\pi x}{L}\right)\sin\left(\frac{\pi y}{H}\right),$$

$$\phi_y = -\frac{3(1-\nu^2)}{\pi^2 E h^3}\left[\frac{L^2H^3}{(L^2+H^2)^2}\right]F\sin\left(\frac{\pi x}{L}\right)\cos\left(\frac{\pi y}{H}\right). \tag{2.7}$$

Now, using eqn. (1.3), the moment components are

$$M_{xx} = -M_{yy} = -\frac{(1-\nu)F}{4}\left[\frac{L^2H^2}{(L^2+H^2)^2}\right]\sin\left(\frac{\pi x}{L}\right)\sin\left(\frac{\pi y}{H}\right),$$

$$M_{xy} = -\frac{F}{4}\left[\frac{LH(\nu L^2+H^2)}{(L^2+H^2)^2}\right]\cos\left(\frac{\pi x}{L}\right)\cos\left(\frac{\pi y}{H}\right), \tag{2.8}$$

$$M_{yx} = \frac{F}{4}\left[\frac{LH(L^2+\nu H^2)}{(L^2+H^2)^2}\right]\cos\left(\frac{\pi x}{L}\right)\cos\left(\frac{\pi y}{H}\right).$$

Finally, differentiating eqn. (2.5) and using eqns. (1.5), one obtains the components of the shear vector

$$V_x = \frac{\pi F}{4}\left[\frac{H}{L^2+H^2}\right]\sin\left(\frac{\pi x}{L}\right)\cos\left(\frac{\pi y}{H}\right), \qquad V_y = \frac{\pi F}{4}\left[\frac{L}{L^2+H^2}\right]\cos\left(\frac{\pi x}{L}\right)\sin\left(\frac{\pi y}{H}\right). \tag{2.9}$$

Note that both the displacement u and the bending moments M_{xy} and M_{yx} are zero on the boundary so that the boundary conditions (2.3) are satisfied.

Now, at the upper right corner of the domain, the normal moment vector $\mathcal{M}_n^- = M_{xx}$ before the corner and $\mathcal{M}_n^+ = M_{yy}$ after the corner are, via the first of eqns. (2.8),

$$\mathcal{M}_n^- = -\mathcal{M}_n^+ = -\frac{(1-\nu)F}{4}\left[\frac{L^2H^2}{(L^2+H^2)^2}\right] \tag{2.10}$$

so that the corner force (at the upper right corner) is

$$\mathcal{M}_n^- - \mathcal{M}_n^+ = -\frac{(1-\nu)F}{2}\left[\frac{L^2H^2}{(L^2+H^2)^2}\right]. \tag{2.11}$$

3. Example in Polar Coordinates

Here a problem in polar coordinates is solved, which problem later will be solved numerically with the cell method. Specifically, below in Fig. 2 is shown the domain of a quarter-annular plate. The distributed load q is zero. The boundaries at $\theta = 0$ and $\theta = \pi/2$ are simply supported, *i.e.*,

$$u = 0\,, \qquad \mathcal{M}_t = 0\,, \tag{3.1}$$

while the inner radius $r = a$ is built in, *i.e.*,

$$u = \phi_t = 0\,. \tag{3.2}$$

A transverse sinusoidal edge traction is applied to the outer radius $r = b$, *viz.,*

$$\mathcal{M}_t = 0\,, \qquad \bar{V}_n = \frac{2F}{b}\sin 4\theta\,, \tag{3.3}$$

where $F > 0$ is the total force of the traction over the interval $\theta \in [\,0\,,\ \pi/4\,]$.

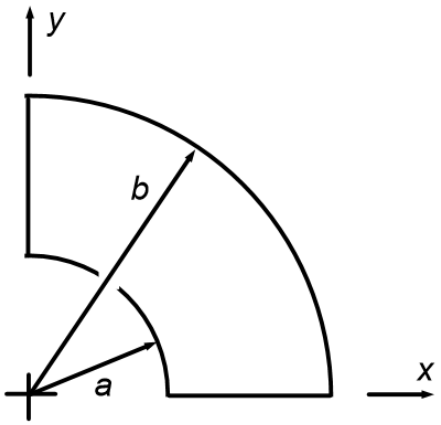

Figure 2. The quarter-annular plate under consideration.

This problem may be solved with a displacement of the form

$$u = f(r)\sin 4\theta\,. \tag{3.4}$$

With eqn. (3.4) and eqns. (1.8), the components of the rotation vector are

$$\phi_r = \frac{4}{r}\,f\cos 4\theta\,, \qquad \phi_\theta = -f'\sin 4\theta\,. \tag{3.5}$$

Next, via eqns. (1.9) and Hooke's Law, the moments are

$$\begin{aligned} M_{rr} &= -M_{\theta\theta} = \frac{Eh^3}{3(1+\nu)}\left(\frac{1}{r}f' - \frac{1}{r^2}f\right)\cos 4\theta, \\ M_{r\theta} &= -\frac{Eh^3}{12(1-\nu^2)}\left(f'' + \frac{\nu}{r}f' - \frac{16\nu}{r^2}f\right)\sin 4\theta, \\ M_{\theta r} &= \frac{Eh^3}{12(1-\nu^2)}\left(\nu f'' + \frac{1}{r}f' - \frac{16}{r^2}f\right)\sin 4\theta\,. \end{aligned} \tag{3.6}$$

Finally, eqn. (1.10) gives the components of the shear vector

$$\begin{aligned} V_r &= -\frac{Eh^3}{12(1-\nu^2)}\left(f''' + \frac{1}{r}f'' - \frac{17}{r^2}f' + \frac{32}{r^3}f\right)\sin 4\theta\,, \\ V_\theta &= -\frac{Eh^3}{3(1-\nu^2)}\left(\frac{1}{r}f'' + \frac{1}{r^2}f' - \frac{16}{r^3}f\right)\cos 4\theta\,. \end{aligned} \tag{3.7}$$

On the boundary, the Kirchhoff shear forces are

$$\begin{aligned} &r = b \ \Rightarrow\ \bar{V}_n = V_r - \frac{1}{r}\frac{\mathrm{d}M_{rr}}{\mathrm{d}\theta}\,, \qquad \theta = 0 \ \Rightarrow\ \bar{V}_n = -V_\theta - \frac{\mathrm{d}M_{\theta\theta}}{\mathrm{d}r}\,, \\ &\theta = \pi/2 \ \Rightarrow\ \bar{V}_n = V_\theta + \frac{\mathrm{d}M_{\theta\theta}}{\mathrm{d}r}\,, \qquad r = a \ \Rightarrow\ \bar{V}_n = -V_r + \frac{1}{r}\frac{\mathrm{d}M_{rr}}{\mathrm{d}\theta}\,, \end{aligned} \tag{3.8}$$

or, respectively, for $r = b$, $\theta = 0$, $\theta = \pi/2$ and $r = a$,

$$\begin{aligned} \bar{V}_n &= -\frac{Eh^3}{12(1-\nu^2)}\left[f''' + \frac{1}{b}f'' - \frac{(33-16\nu)}{b^2}f' + \frac{16(3-\nu)}{b^3}f\right]\sin 4\theta\,, \\ \bar{V}_n &= \frac{Eh^3}{12(1-\nu^2)}\left[\frac{4(2-\nu)}{r}f'' - \frac{4(1-2\nu)}{r^2}f' - \frac{8(7+\nu)}{r^3}f\right], \\ \bar{V}_n &= -\frac{Eh^3}{12(1-\nu^2)}\left[\frac{4(2-\nu)}{r}f'' - \frac{4(1-2\nu)}{r^2}f' - \frac{8(7+\nu)}{r^3}f\right], \\ \bar{V}_n &= \frac{Eh^3}{12(1-\nu^2)}\left[f''' + \frac{1}{a}f'' - \frac{(33-16\nu)}{a^2}f' + \frac{16(3-\nu)}{a^3}f\right]\sin 4\theta\,. \end{aligned} \tag{3.9}$$

Now, substituting the displacement (3.4) into the governing equation $\nabla^4 u = 0$, see eqn. (1.11), one obtains the differential equation

$$f'''' + \frac{2}{r} f''' - \frac{33}{r^2} f'' + \frac{33}{r^3} f' + \frac{192}{r^4} f = 0 \,. \tag{3.10}$$

The solution to eqn. (3.10) is

$$\begin{aligned} f &= \frac{k_1}{r^4} + \frac{k_2}{r^2} + k_3 r^4 + k_4 r^6 \,, \\ f' &= -4\frac{k_1}{r^5} - 2\frac{k_2}{r^3} + 4k_3 r^3 + 6k_4 r^5 \,, \\ f'' &= 20\frac{k_1}{r^6} + 6\frac{k_2}{r^4} + 12k_3 r^2 + 30k_4 r^4 \,, \\ f''' &= -120\frac{k_1}{r^7} - 24\frac{k_2}{r^5} + 24k_3 r + 120k_4 r^3 \,. \end{aligned} \tag{3.11}$$

Looking at eqns. (3.4) and (3.6), one sees that the boundary conditions (3.1) are satisfied identically. The conditions, respectively, $u(a,\theta) = 0$, $\phi_t = -\phi_\theta(a,\theta) = 0$, $\mathcal{M}_t = M_{r\theta}(b,\theta) = 0$ and $\bar{V}_n = (2F/b)\sin 4\theta$ yield the system of equations to satisfy the boundary conditions (3.2) and (3.3), *viz.,*

$$\begin{bmatrix} 1/a^4 & 1/a^2 & a^4 & a^6 \\ -2/a^5 & -1/a^3 & 2a^3 & 3a^5 \\ 10(1-\nu)/b^6 & 3(1-3\nu)/b^4 & 6(1-\nu)b^2 & 5(3-\nu)b^4 \\ -5(1-\nu)/b^6 & -3(2-\nu)/b^4 & 3(1-\nu)b^2 & -5\nu b^4 \end{bmatrix} \begin{bmatrix} k_1 \\ k_2 \\ k_3 \\ k_4 \end{bmatrix} = \begin{bmatrix} 0 \\ 0 \\ 0 \\ 3(1-\nu^2)F/(2Eh^3) \end{bmatrix} . \tag{3.12}$$

Using the constants

$$E = 3.0 \times 10^7 \text{ psi} \,, \quad \nu = 0.3 \,, \quad h = 1.0 \text{ in} \,, \quad F = 10\,000 \text{ lb} \,, \quad a = 120 \text{ in} \,, \quad b = 360 \text{ in} \,, \tag{3.13}$$

the solution to eqn. (3.12) is

$$\begin{aligned} k_1 &= 1.666\,591\,940\,231\,4806 \times 10^8 \,, & k_2 &= -1.547\,802\,450\,020\,5023 \times 10^4 \,, \\ k_3 &= 1.354\,435\,354\,756\,7996 \times 10^{-9} \,, & k_4 &= -3.252\,532\,373\,598\,9290 \times 10^{-15} \,, \end{aligned} \tag{3.14}$$

which constants solve the problem at hand.

As a final comment, for the constants (3.13) and (3.14), the values of the four corner forces are

Corner Force at (r,θ)	Value (lb)
$(M_{\theta\theta} - M_{rr})(a,0)$	0
$(M_{\theta\theta} - M_{rr})(b,0)$	−3935.94
$(M_{rr} - M_{\theta\theta})(b,\pi/2)$	3935.94
$(M_{rr} - M_{\theta\theta})(a,\pi/2)$	0

4. Interpolations for the Cell Method

The cell method uses the two-dimensional bi-quadratic differentiation cell depicted below in Figs. 3 and 4. With the aid of the quadratic functions

$$f^0(s) = \frac{1}{2}(-s + s^2) \,, \qquad f^1(s) = 1 - s^2 \,, \qquad f^2(s) = \frac{1}{2}(s + s^2) \,, \qquad s \in (-1,1) \tag{4.1}$$

one may construct the nine interpolation functions S^I for the cell via the tensor product

$$\begin{matrix} S^0 = f^0(\xi_0)f^0(\xi_1) & S^1 = f^1(\xi_0)f^0(\xi_1) & S^2 = f^2(\xi_0)f^0(\xi_1) \\ S^3 = f^0(\xi_0)f^1(\xi_1) & S^4 = f^1(\xi_0)f^1(\xi_1) & S^5 = f^2(\xi_0)f^1(\xi_1) \\ S^6 = f^0(\xi_0)f^2(\xi_1) & S^7 = f^1(\xi_0)f^2(\xi_1) & S^8 = f^2(\xi_0)f^2(\xi_1) \end{matrix} \quad , \qquad \xi_i \in (-1,1) \ . \tag{4.2}$$

Note that these nine functions correspond to the nine "shape functions" of the LaGrange bi-quadratic finite element. Notwithstanding, the mapping of the differentiation cell from **ξ**–space to **x**–space is

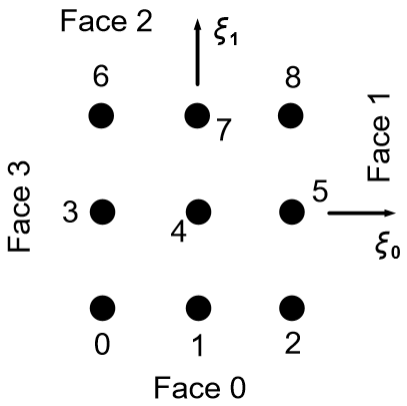

Figure 3. Differentiation cell in normalized **ξ**–space.

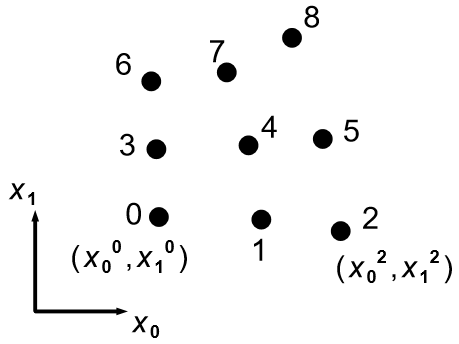

Figure 4. Differentiation cell in (physical) **x**–space.

achieved via

$$x_i = S^I x_i^I \ , \tag{4.3}$$

where x_i^I are the coordinates of the cell's points (see Fig. 4). The differentials of eqn. (4.3) are then

$$\mathrm{d}x_i = A_{i\alpha}\mathrm{d}\xi_\alpha \ , \qquad A_{i\alpha} = \frac{\partial x_i}{\partial \xi_\alpha} = S^I_{,\alpha} x_i^I \ , \qquad A_{i\alpha,\beta} = S^I_{,\alpha\beta} x_i^I \ , \tag{4.4}$$

and

$$\mathrm{d}\xi_\alpha = A^{-1}_{\alpha i}\mathrm{d}x_i \ , \qquad A^{-1}_{\alpha i} = \frac{\partial \xi_\alpha}{\partial x_i} \ . \tag{4.5}$$

Now, with the derivative

$$\frac{\partial A^{-1}_{\gamma j}}{\partial \xi_\beta} = -A^{-1}_{\gamma i} A_{i\alpha,\beta} A^{-1}_{\alpha j} \ , \tag{4.6}$$

one finds that the physical gradients of the interpolation functions are, which are obtained via the Chain Rule,

$$S^I_{,j} = S^I_{,\alpha} A^{-1}_{\alpha j} \ , \qquad S^I_{,jk} = \left(S^I_{,\gamma\beta} - S^I_{,\alpha} A_{i\gamma,\beta} A^{-1}_{\alpha i}\right) A^{-1}_{\beta k} A^{-1}_{\gamma j} \ . \tag{4.7}$$

Thus, a field variable g and its physical gradients may be interpolated within the cell as

$$g = S^I g^I \ , \qquad g_{,i} = S^I_{,i} g^I \ , \qquad g_{,ij} = S^I_{,ij} g^I \ , \tag{4.8}$$

where g^I are the values of the field variable at the cell's points.

To calculate the Kirchhoff force on the boundary, the boundary differentiation segments pictured below in Figs. 5 and 6 are used. On the boundary, the mapping from normalized s–space to (physical) t–space is done via, similarly to eqn. (4.3),

$$x_i = f^I x_i^I \ , \tag{4.9}$$

where the three functions $f^I(s)$ are as in eqns. (4.1) and x_i^I are the coordinates of the boundary segment's points. Note that, depending on which face (in Fig. 3) the boundary segment belongs to, the points in Figs. 3 and 4 need to be renumbered as per Figs. 5 and 6. Nonetheless, the differential of eqn. (4.9) is

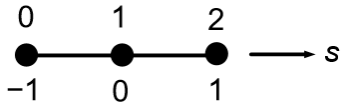

Figure 5. Boundary differentiation segment in normalized s–space.

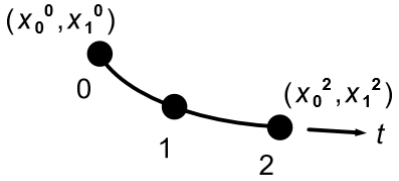

Figure 6. Boundary differentiation segment in (physical) t–space.

$$\mathrm{d}x_i = b_i \mathrm{d}s \ , \qquad b_i = f^I_{,s} x_i^I \ , \tag{4.10}$$

and

$$(\mathrm{d}t)^2 = \mathrm{d}x_i \mathrm{d}x_i = b_i b_i (\mathrm{d}s)^2 \quad \Rightarrow \quad \mathrm{d}t = b\mathrm{d}s \ , \qquad b = \sqrt{b_i b_i} \ . \tag{4.11}$$

Consequently, via the Chain Rule,

$$f^I_{,t} = \frac{1}{b} f^I_{,s} \tag{4.12}$$

so that a field variable g and its tangential derivative may be interpolated along the boundary segment as

$$g = f^I g^I \ , \qquad g_{,t} = f^I_{,t} g^I \ . \tag{4.13}$$

5. The Cell Method

Denote the normalized shear vector v_i and the normalized moment tensor m_{ij} as

$$v_i = \frac{V_i}{D} \ , \qquad m_{ij} = \frac{M_{ij}}{D} \ , \tag{5.1}$$

where D is as in eqn. (1.3). Instead of using the fourth-order eqn. (1.7) directly, write the governing equations of classical plate theory as the six equations

$$\mathbf{w} = \begin{bmatrix} v_x \\ v_y \\ m_{xx} \\ m_{xy} \\ m_{yx} \\ u \end{bmatrix}$$

Figure 7. Vector of the nodal degrees of freedom.

$$\begin{aligned} v_x &= m_{xy,x} - m_{xx,y} \\ v_y &= -m_{xx,x} - m_{yx,y} \\ m_{xx} &= (1-\nu) u_{,xy} \\ m_{xy} &= -u_{,xx} - \nu u_{,yy} \\ m_{yx} &= \nu u_{,xx} + u_{,yy} \\ v_{,x} + v_{,y} &= -q/D \ , \end{aligned} \tag{5.2}$$

which are merely, respectively, eqns. (1.5), (1.3) with (1.2), and (1.6) of Sec. 1. Each point (or node) of the differentiation cell of Fig. 4 then has six degrees-of-freedom, as pictured at above left in Fig. 7. Now, interpolate the field variables with the functions (4.2):

$$v_i = S^J v_i^J \ , \qquad m_{ij} = S^J m_{ij}^J \ , \qquad u = S^J u^J \ , \tag{5.3}$$

where, respectively, v_i^J, m_{ij}^J and u^J are the nodal values of the normalized shear vector, normalized moment tensor, and transverse displacement. Next, use the physical gradients of the interpolation functions to represent the derivatives in eqns. (5.2). Thus, the interpolated versions of eqns. (5.2), evaluated at point I, are

$$\begin{aligned} &v_x^I - S(I)_{,x}^J m_{xy}^J + S(I)_{,y}^J m_{xx}^J = 0 \\ &v_y^I + S(I)_{,x}^J m_{xx}^J + S(I)_{,y}^J m_{yx}^J = 0 \\ &m_{xx}^I - (1-\nu) S(I)_{,xy}^J u^J = 0 \\ &m_{xy}^I + \left[S(I)_{,xx}^J + \nu S(I)_{,yy}^J \right] u^J = 0 \\ &m_{yx}^I - \left[\nu S(I)_{,xx}^J + S(I)_{,yy}^J \right] u^J = 0 \\ &S(I)_{,x}^J v_x^J + S(I)_{,y}^J v_y^J = -q^I/D \ , \end{aligned} \tag{5.4}$$

where $S(I)^J$ means S^J evaluated at point I. Now, write the six eqns. (5.4) at point I in terms of matrices

$$\left[\mathbf{G}^0 \quad \mathbf{G}^1 \quad \mathbf{G}^2 \quad \ldots \quad \mathbf{G}^7 \quad \mathbf{G}^8 \right] \begin{bmatrix} \mathbf{w}^0 \\ \mathbf{w}^1 \\ \mathbf{w}^2 \\ \vdots \\ \mathbf{w}^7 \\ \mathbf{w}^8 \end{bmatrix} = \mathbf{r} \ , \tag{5.5}$$

which notation will be convenient for prescribing the boundary conditions, and will be described later below. In eqns. (5.5), each $\mathbf{G}^J$ is a 6×6 matrix, each $\mathbf{w}^J$ is a 6×1 matrix, and $\mathbf{r}$ also is a 6×1 matrix.

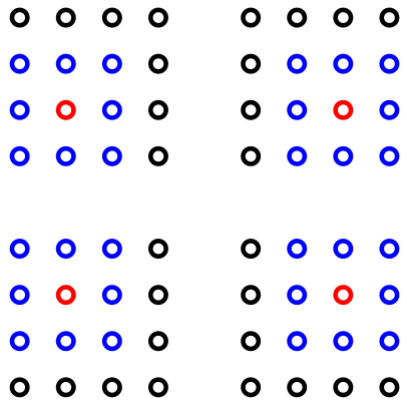

Figure 8. Four copies of a computational grid as explained in the text.

The computational procedure of the cell method is as follows. Consider the 4×4 computational grid of points shown at above right in Fig. 8, which grid possesses 96 degrees of freedom. The grid consists of four (overlapping) differentiation cells (shown in red and blue). At each of the internal (red) points, equations (5.5) are evaluated at node 4 of each cell. For points on the boundary (that are not a corner of the domain), eqns. (5.5) are evaluated at either points 1, 3, 5 or 7 of each cell (as appropriate). Finally, at the corner points, eqns. (5.5) are evaluated at either points 0, 2, 6 or 8 of each cell (again, as appropriate). At this juncture, a 96×96 system of algebraic equations has been generated, but the system will be rank-deficient by 24 equations (*i.e.,* by two equations for each boundary point). This rank-deficiency is removed by applying the boundary conditions for the problem.

Before applying the boundary conditions, each boundary node needs to be transformed to the boundary nt–system. Consequently, the normalized shear components in the nt–system are

$$v_n = n_i v_i \ , \qquad v_t = t_i v_i \ , \tag{5.6}$$

where n_i and t_i are the components of the boundary unit vectors $\mathbf{n}$ and $\mathbf{t}$. Equivalently, eqn. (5.6) is

$$\begin{bmatrix} v_n \\ v_t \end{bmatrix} = \begin{bmatrix} n_x & n_y \\ t_x & t_y \end{bmatrix} \begin{bmatrix} v_x \\ v_y \end{bmatrix} \equiv \mathbf{R} \begin{bmatrix} v_x \\ v_y \end{bmatrix} \ . \tag{5.7}$$

Similarly, the normalized moment components are in the nt–system,

$$m_{nn} = n_i m_{ij} n_j \ , \qquad m_{nt} = n_i m_{ij} t_j \ , \qquad m_{tn} = t_i m_{ij} n_j \ , \tag{5.8}$$

or equivalently,

$$\begin{bmatrix} m_{nn} \\ m_{nt} \\ m_{tn} \end{bmatrix} = \begin{bmatrix} n_x^2 - n_y^2 & n_x n_y & n_x n_y \\ n_x t_x - n_y t_y & n_x t_y & t_x n_y \\ n_x t_x - n_y t_y & t_x n_y & n_x t_y \end{bmatrix} \begin{bmatrix} m_{xx} \\ m_{xy} \\ m_{yx} \end{bmatrix} \equiv \mathbf{T} \begin{bmatrix} m_{xx} \\ m_{xy} \\ m_{yx} \end{bmatrix} . \tag{5.9}$$

Equations (5.7) and (5.9) can then be combined into the nodal transformation formulas shown below in Figs. 9 and 10. Now, say that eqn. (5.5) is for a cell point $I \neq 1$ and that point $J = 1$ of the cell is on the

$$\mathbf{w}_{\mathrm{xy}} = \begin{bmatrix} v_x \\ v_y \\ m_{xx} \\ m_{xy} \\ m_{yx} \\ u \end{bmatrix} \qquad \mathbf{w}_{\mathrm{nt}} = \begin{bmatrix} v_n \\ v_t \\ m_{nn} \\ m_{nt} \\ m_{tn} \\ u \end{bmatrix} \qquad \mathbf{U} = \begin{bmatrix} \mathbf{R} & \mathbf{0} & \mathbf{0} \\ \mathbf{0} & \mathbf{T} & \mathbf{0} \\ \mathbf{0} & \mathbf{0} & 1 \end{bmatrix} , \qquad \mathbf{w}_{\mathrm{nt}} = \mathbf{U}\,\mathbf{w}_{\mathrm{xy}} , \qquad \mathbf{w}_{\mathrm{xy}} = \mathbf{U}^{-1}\mathbf{w}_{\mathrm{nt}}$$

Figure 9. The degrees-of-freedom for a computational node in the xy– and nt–systems.

Figure 10. Nodal transformation formulas between the xy– and nt–systems.

boundary, *i.e.,* it is in the boundary nt–system. Then eqn. (5.5) becomes

$$\left[\, \mathbf{G}^0 \quad \mathbf{G}^1\mathbf{U}^{-1} \quad \mathbf{G}^2 \quad \dots \quad \mathbf{G}^7 \quad \mathbf{G}^8 \,\right] \begin{bmatrix} \mathbf{w}_{\mathrm{xy}}^0 \\ \mathbf{w}_{\mathrm{nt}}^1 \\ \mathbf{w}_{\mathrm{xy}}^2 \\ \vdots \\ \mathbf{w}_{\mathrm{xy}}^7 \\ \mathbf{w}_{\mathrm{xy}}^8 \end{bmatrix} = \mathbf{r} . \tag{5.10}$$

Finally, in the case that eqn. (5.5) is for a cell point $I = 1$ on the boundary, then eqn. (5.5) is

$$\left[\, \mathbf{U}\mathbf{G}^0 \quad \mathbf{U}\mathbf{G}^1\mathbf{U}^{-1} \quad \mathbf{U}\mathbf{G}^2 \quad \dots \quad \mathbf{U}\mathbf{G}^7 \quad \mathbf{U}\mathbf{G}^8 \,\right] \begin{bmatrix} \mathbf{w}_{\mathrm{xy}}^0 \\ \mathbf{w}_{\mathrm{nt}}^1 \\ \mathbf{w}_{\mathrm{xy}}^2 \\ \vdots \\ \mathbf{w}_{\mathrm{xy}}^7 \\ \mathbf{w}_{\mathrm{xy}}^8 \end{bmatrix} = \mathbf{U}\mathbf{r} . \tag{5.11}$$

The procedure for applying the boundary conditions is as follows. If the rotation ϕ_t is known, then equation number 3 (concerning m_{nt}, *cf.,* Fig. 9) at the boundary point I is replaced with

$$t_i^I \varepsilon_{ij} S(I)_{,j}^J u^J = \phi_t^I , \tag{5.12}$$

which follows from eqn. (1.1) and $\phi_t = t_i \phi_i$. If the Kirchhoff force $\bar{V}_n$ is known, then equation number 5 (concerning u) at the boundary point I is replaced with

$$v_n^I - f(I)_{,t}^J m_{nn}^J = \bar{v}_n^I = \bar{V}_n^I / D , \tag{5.13}$$

which follows from $\bar{V}_n = V_n - \mathcal{M}_{n,t}$ and $\mathcal{M}_n = M_{nn}$. Note that in eqn. (5.13), the functions $f_{,t}^J$ are as per eqn. (4.12) so that J is summed from 0 to 2 (for the points on the boundary differentiation segment, *cf.,* Fig 6). Once the conditions (5.12) and (5.13) have been applied, prescribing that any nodal values of u^I and/or $\mathcal{M}_t^I / D = m_{nt}^I$ are known can be enforced by appropriate algebraic rearrangement of the (global) system of equations.

It should be noted that, while the resulting system of algebraic equations is banded, during their solution, row interchanges are required (which is not the case, *e.g.,* in the finite element method).

6. Numerical Example in Rectangular Coordinates

Here the problem solved analytically in Sec. 2 is solved numerically with the cell method. Due to symmetry, only the upper right quadrant of Fig. 1 needs to be analyzed, so that the boundary conditions are

$$\text{on } x = 0 \text{ and } y = 0\,, \quad \phi_t = \bar{V}_n = 0\ ; \qquad \text{on } x = \frac{L}{2} \text{ and } y = \frac{H}{2}\,, \quad u = \mathcal{M}_t = 0\ . \tag{6.1}$$

The values of the constants used in the analysis are

$$L = 360 \text{ in}\,, \quad H = 240 \text{ in}\,, \quad F = 10000 \text{ lb}\,, \quad E = 3 \times 10^7 \text{ psi}\,, \quad \nu = 0.3\,, \quad h = 1.0 \text{ in}\,. \tag{6.2}$$

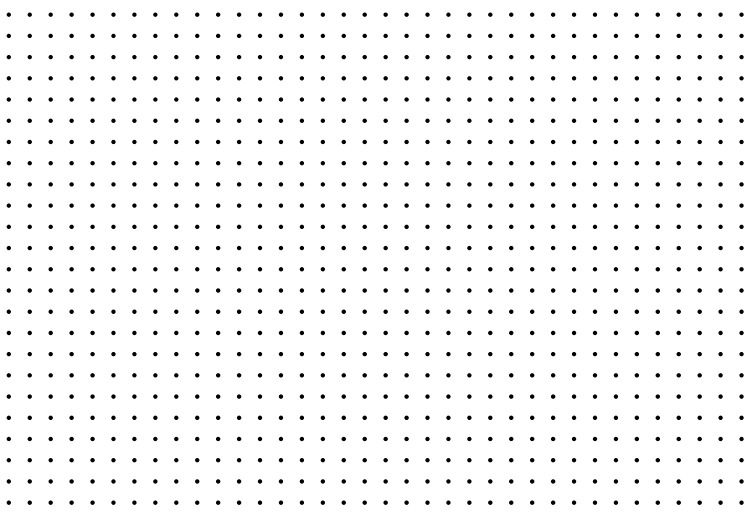

Figure 11. Computational grid used in the analysis.

The computational grid used is shown above in Fig. 11. It consists of a 36×24 array of 864 points, and a 34×22 array of 748 (overlapping) differentiation cells. Also, due to the $\bar{V}_n$ boundary conditions, on the face $x = 0$ there are 22 (overlapping) boundary differentiation segments; and on $y = 0$, 34 (overlapping) boundary differentiation segments.

In the graphs of Figs. 12 through 21 which follow, the solid curves are from the exact analytical solution, and the plotted points are from the numerical calculations.

Figures 12 and 13 below show, respectively, the displacement u and rotation component ϕ_x along the left boundary of the analyzed domain $x = 0$. For all practical purposes, these two numerically calculated quantities basically coincide with the exact solution.

The same thing can be said for the numerically calculated displacement u and rotation vector ϕ_i along the vertical line of grid points located at $x = 92.5714$ in shown, respectively, in Figs. 14 and 15 below.

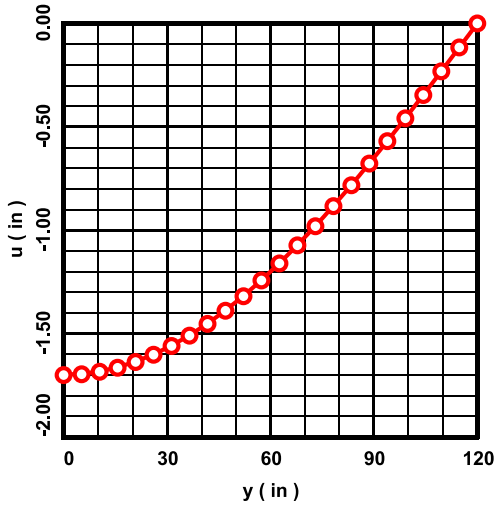

Figure 12. The displacement u at $x = 0$.

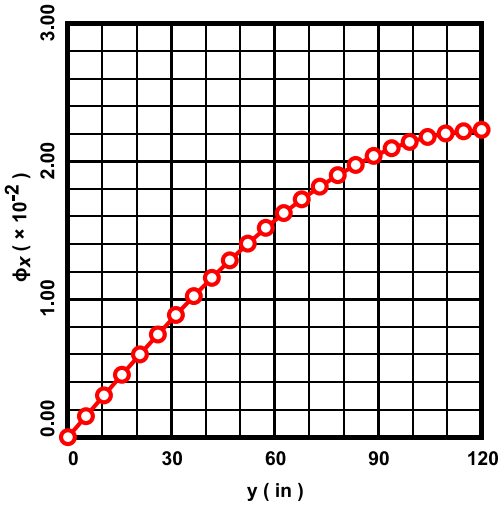

Figure 13. The rotation component ϕ_x at $x = 0$.

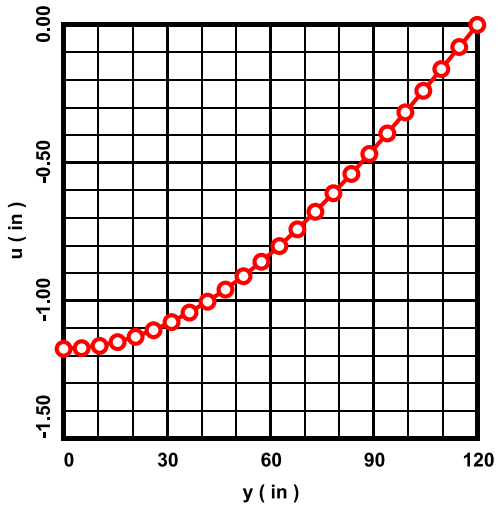

Figure 14. The displacement u at $x = 92.5714$ in.

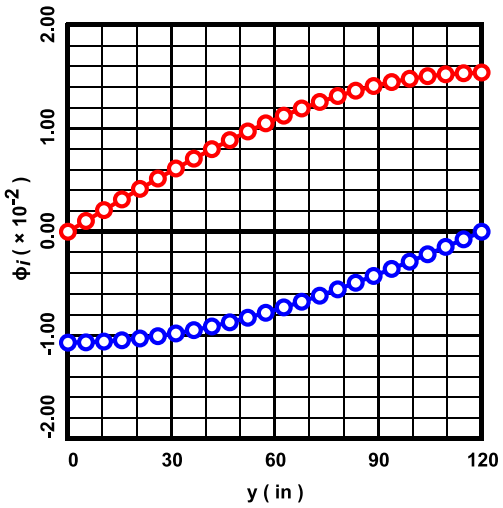

Figure 15. The rotation components ϕ_x (red) and ϕ_y (blue) at $x = 92.5714$ in.

Figure 16 below shows the results for the moment components M_{xy} and M_{yx} at the left boundary of the analyzed domain $x = 0$. Except for the slight error in M_{xy} at the top boundary $y = H/2$, the numerical results are highly accurate. The reason for this slight error in M_{xy} is not clear to the author. Nevertheless, along this same boundary, the numerical results for the shear component V_y is accurate everywhere, as is seen from Fig. 17 below.

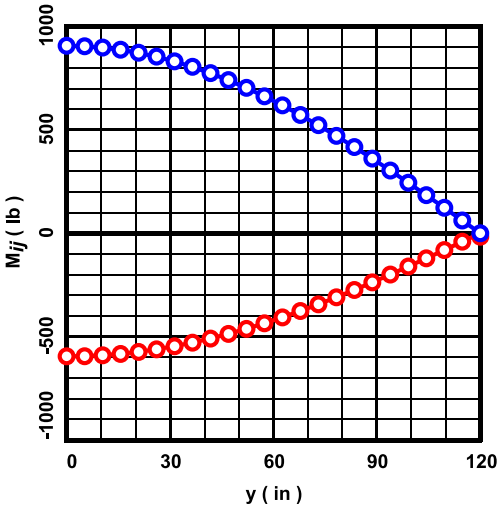

Figure 16. Moment components M_{xy} (red) and M_{yx} (blue) at $x = 0$.

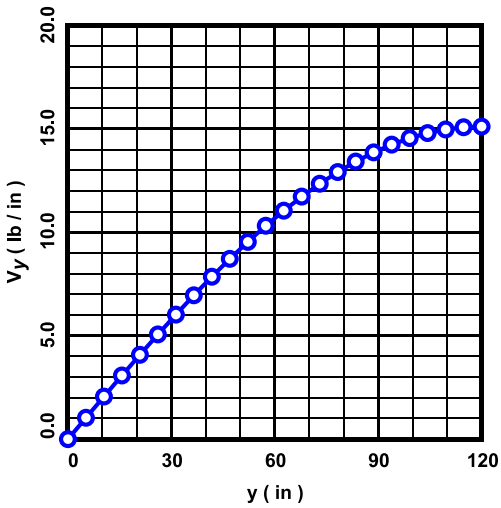

Figure 17. Shear component V_y at $x = 0$.

Directly below, in Fig. 18, is shown the numerically calculated results for the moment component M_{xx} along the right boundary of the domain $x = 180$ in. The numerical results are highly accurate. Figure 19 at below right shows the results for the shear component V_x along the same boundary. Similarly to the results for M_{xy} in Fig. 16, there is a slight error in the calculated value of V_x at the upper boundary of the domain. But, elsewhere, the numerical results are accurate. Again, the author does not know the reason for this slight error.

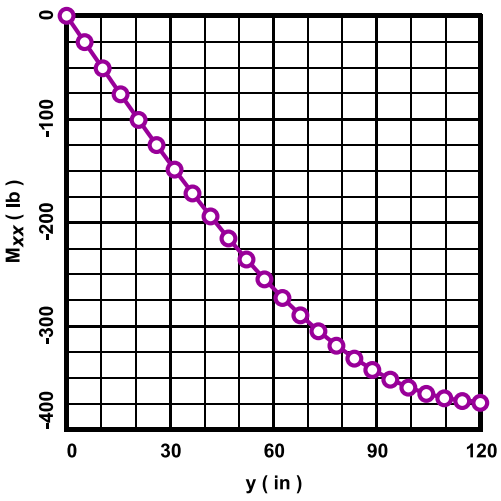

Figure 18. Moment component M_{xx} at $x = 180$ in.

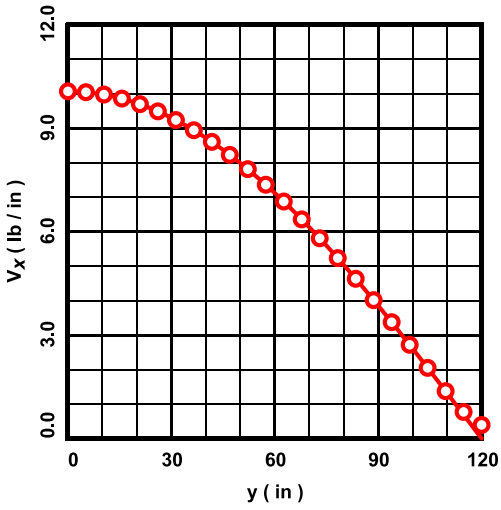

Figure 19. Shear component V_x at $x = 180$ in.

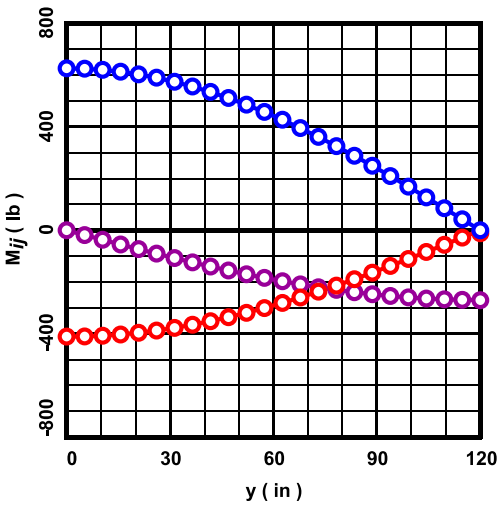

Figure 20. Moment components M_{xy} (red), M_{yx} (blue) and M_{xx} (purple) at $x = 92.5714$ in.

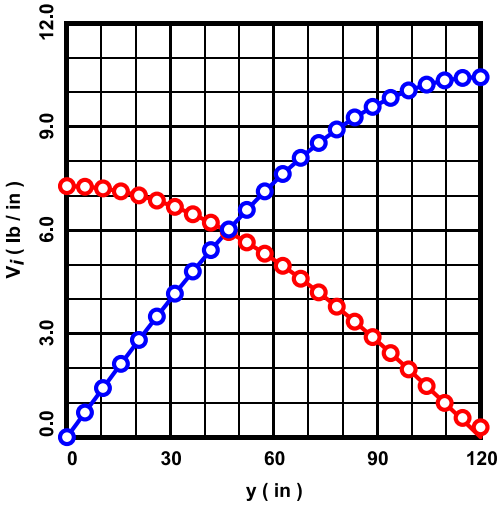

Figure 21. Shear components V_x (red) and V_y (blue) at $x = 92.5714$ in.

Figures 20 and 21 directly above show the numerical results for the moment components M_{ij} and shear components V_i along the vertical line of grid points located at $x = 92.5714$ in. Again, all the numerical results are highly accurate, except for slight errors in M_{xy} and V_x at the top boundary of the domain.

Finally, at the upper right corner of the domain, the numerically calculated corner force is -748.528 lb, compared to the exact value -745.562 lb. This amounts to 0.398% relative error.

For this problem, except for a few very slight errors in the stress resultants on the boundary, the cell method performs quite admirably.

7. Numerical Example in Polar Coordinates

In this section, the problem solved analytically in Sec. 3 is solved numerically with the cell method. The boundary conditions for this problem were stated previously in eqns. (3.1) through (3.3), and the constants used were given previously in eqn. (3.13).

The computational grid used in the analysis is shown below in Fig. 22. The grid consists of a 25 (radial) × 37 (circumferential) array of 925 points, and a 23 (radial) × 35 (circumferential) array of 805 (overlapping) differentiation cells. Also, due to the prescribed values of $\bar{V}_n$, the outer radius of the domain is spanned by 35 (overlapping) boundary differentiation segments.

As in the previous section, in the graphs of Figs. 23 through 39 below, the solid curves are from the exact analytical solution; and the plotted points, from the numerical solution.

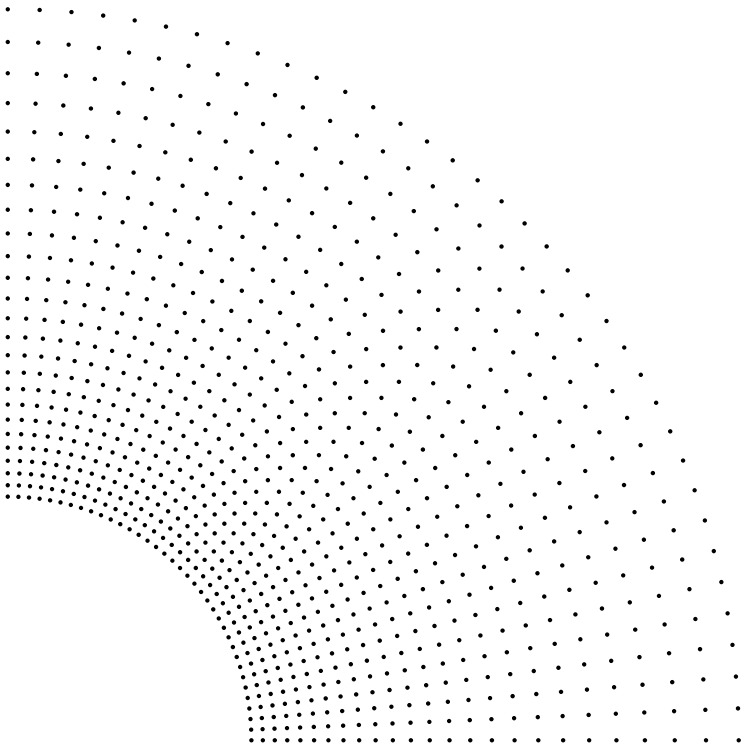

Figure 22. Computational grid used in the analysis.

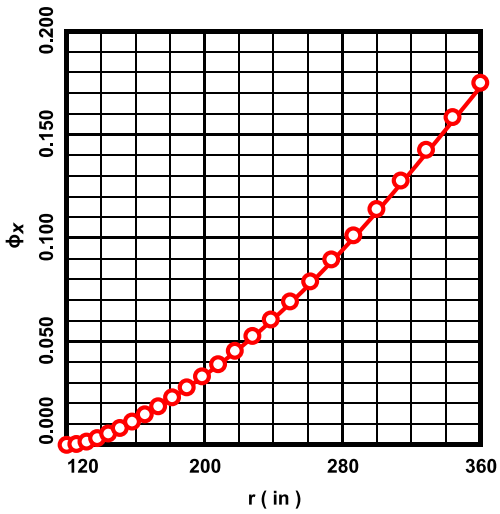

Figure 23. Rotation component ϕ_x at $\theta = 0$.

At left, in Fig. 23, is shown the numerical results for the rotation component ϕ_x along the bottom boundary of the domain at $\theta = 0$. As is evident, the magnitude of this numerically calculated rotation component is (very slightly) overestimated.

Below, in Figs. 24 and 25, respectively, are shown the results of the calculation for the displacement u and rotation vector ϕ_i at the outer radius of the domain $r = b$. Here, all the numerically calculated results basically coincide with the exact solution.

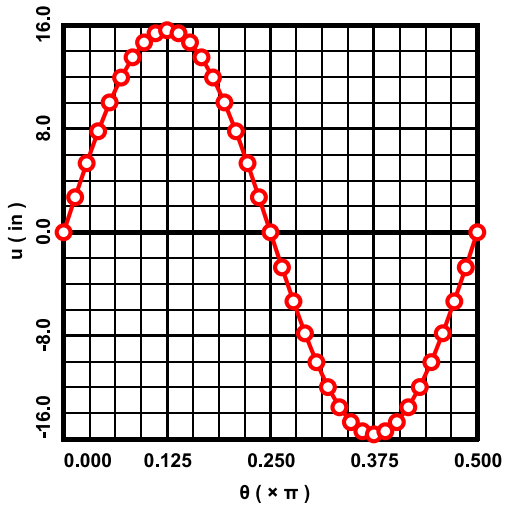

Figure 24. The displacement u at $r = b$.

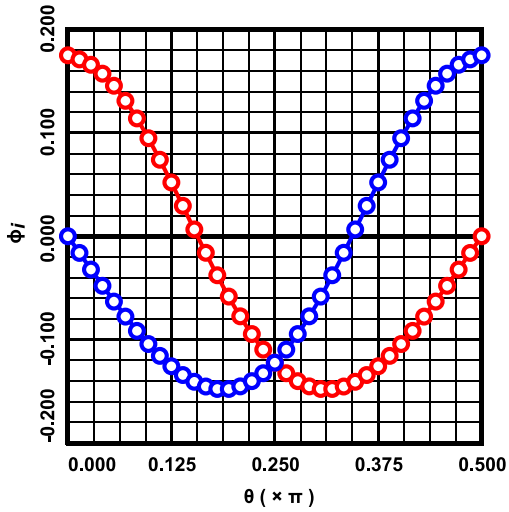

Figure 25. Rotation components ϕ_x (red) and ϕ_y (blue) at $r = b$.

As was the case for Figs. 24 and 25, the numerically calculated displacement u and rotation vector ϕ_i along the radial line of grid points located at $\theta = \pi/8$, shown, respectively, in Figs. 26 and 27 below, are highly accurate.

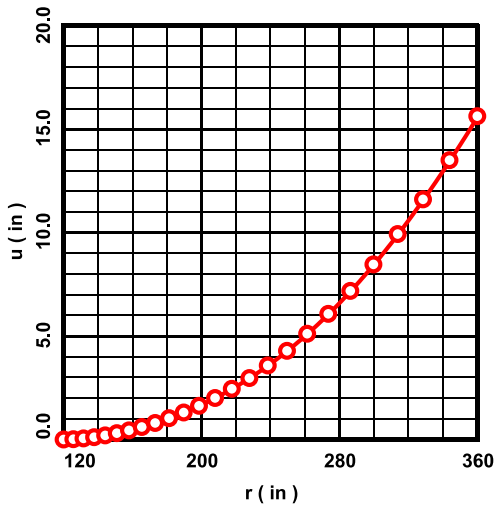

Figure 26. The displacement u at $\theta = \pi/8$.

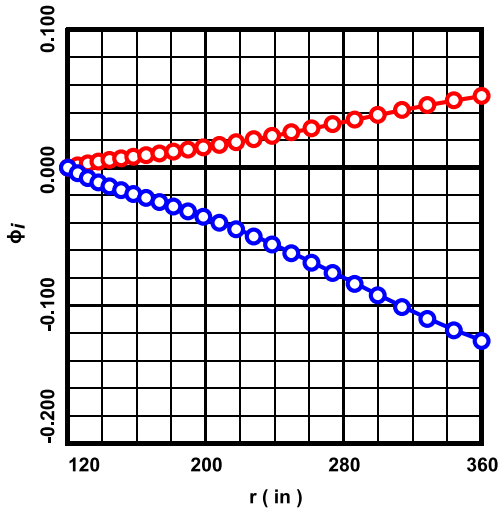

Figure 27. Rotation components ϕ_x (red) and ϕ_y (blue) at $\theta = \pi/8$.

The same thing can be said for the displacement u and rotation vector ϕ_i along the circumferential ring of grid points located at $r = 238.442$ in, shown below, respectively, in Figs. 28 and 29.

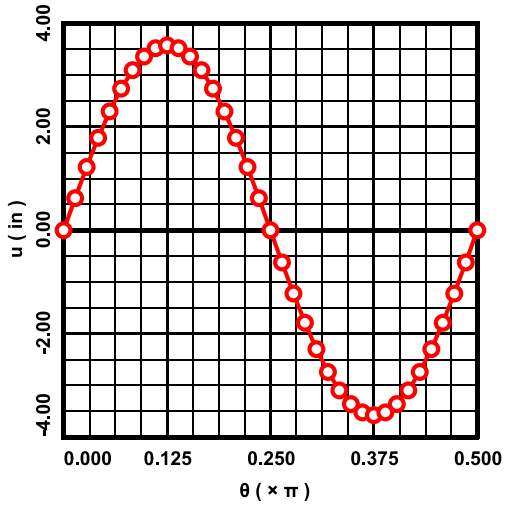

Figure 28. The displacement u at $r = 238.442$ in.

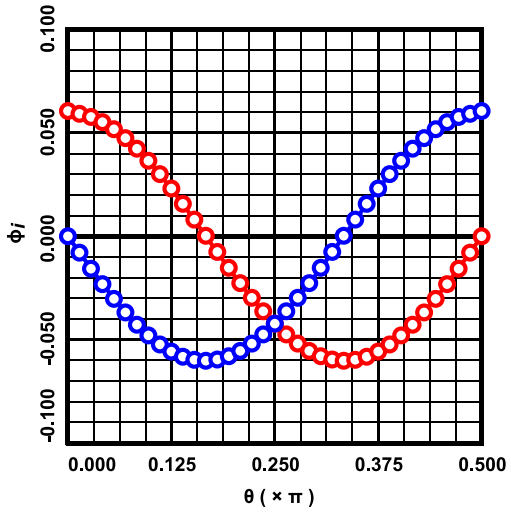

Figure 29. Rotation components ϕ_x (red) and ϕ_y (blue) at $r = 238.442$ in.

Figure 30, at below left, shows the numerical results for the moment component M_{xx} along the bottom boundary of the domain located at $\theta = 0$. As was the case for ϕ_x at $\theta = 0$ in Fig. 23, here the numerically calculated magnitude of M_{xx} is (very slightly) overestimated. Along the same boundary, as shown at below right in Fig. 31, the numerically calculated values for the shear component V_y are highly accurate, except for a slight error at the outer radius of the domain. The author does not know why this (slight) error occurs.

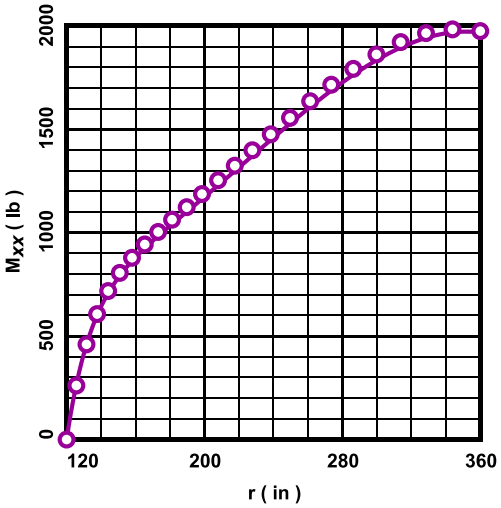

Figure 30. Moment component M_{xx} at $\theta = 0$.

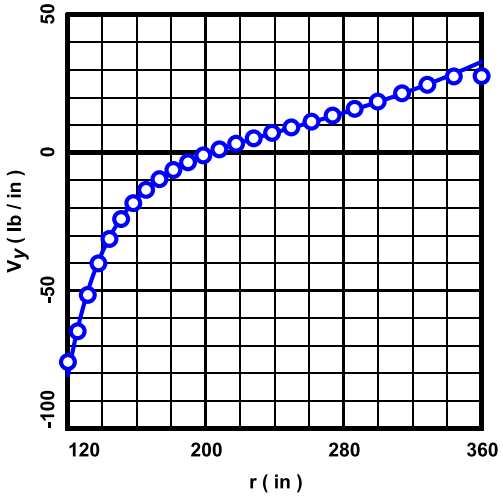

Figure 31. Shear component V_y at $\theta = 0$.

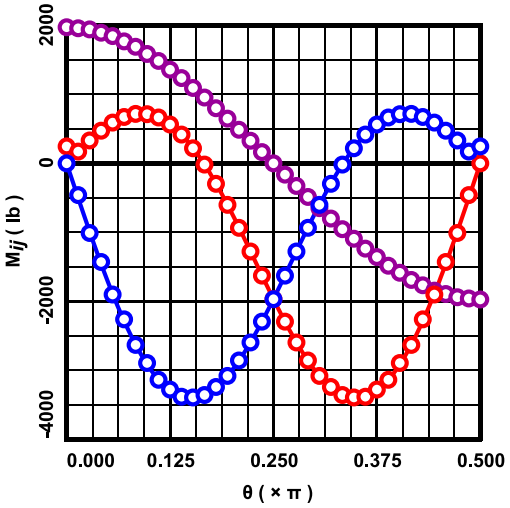

Figure 32. Moment components M_{xy} (red), M_{yx} (blue) and M_{xx} (purple) at $r = b$.

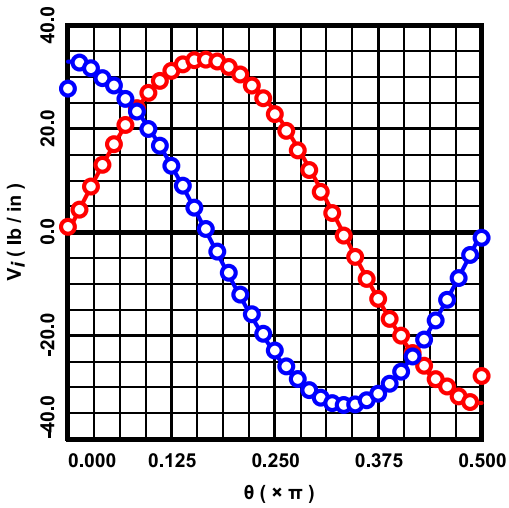

Figure 33. Shear components V_x (red) and V_y (blue) at $r = b$.

Figure 32, at above left, shows the numerically calculated values for the moment components M_{ij} at the outer radius of the domain $r = b$. All the numerical results are quite accurate, except for two data points, *viz.,* M_{xy} at $\theta = 0$, and M_{yx} at $\theta = \pi/2$. These two errors appear to be due to how the boundary conditions were applied at these two points. At the corner $(r, \theta) = (b, 0)$, the simply supported conditions $u = \mathcal{M}_t = 0$ of the bottom face were applied; and at the corner $(r, \theta) = (b, \pi/2)$, the simply supported conditions of the left face were applied. The same kind of thing occurs in Fig. 33, at above right, concerning the shear vector V_i, where all the numerical results are accurate, except for the two data points at $(r, \theta) = (b, 0)$ for V_x, and at $(r, \theta) = (b, \pi/2)$ for V_y. It would be worthwhile to look into if the calculational code could be modified to allow for specification of four boundary conditions (instead of just two) at the corner points, *i.e.,* two boundary conditions for each adjoining face.

Figure 34 below shows the numerically calculated moment components M_{ij} along the inner radius of the domain at $r = a$, which numerical values are highly accurate. Figure 35 below shows the results, also at the inner radius, for the shear vector V_i. Overall, the results for the numerically calculated shear components are acceptably accurate, although the magnitudes of these components are underestimated somewhat.

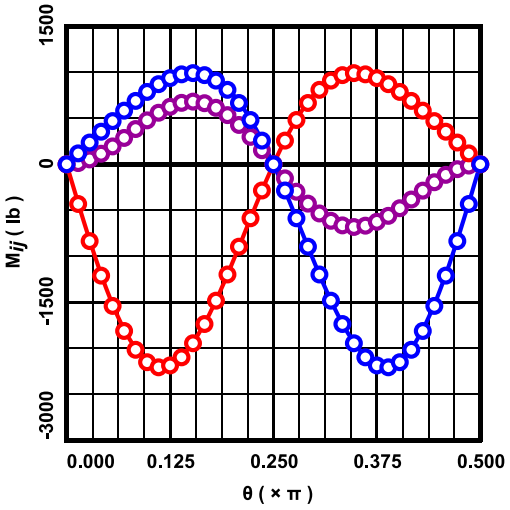

Figure 34. Moment components M_{xy} (red), M_{yx} (blue) and M_{xx} (purple) at $r = a$.

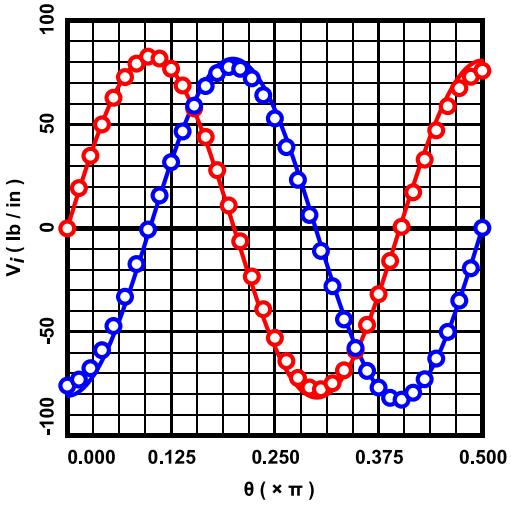

Figure 35. Shear components V_x (red) and V_y (blue) at $r = a$.

The results of the numerical calculations for the moment components M_{ij} and the shear vector V_i, along the radial line of grid points located at $\theta = \pi/8$, are shown below, respectively, in Figs. 36 and 37. Here, all the numerical results are highly accurate.

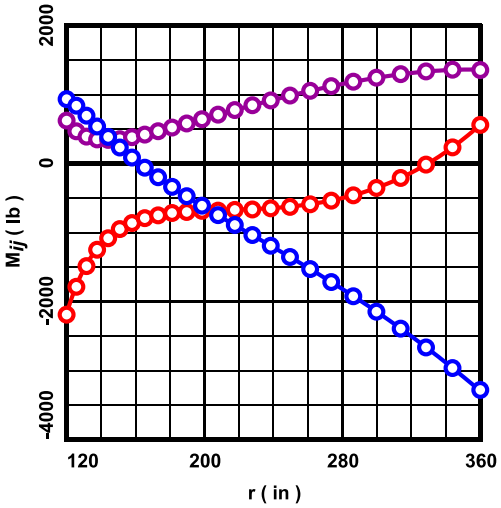

Figure 36. Moment components M_{xy} (red), M_{yx} (blue) and M_{xx} (purple) at $\theta = \pi/8$.

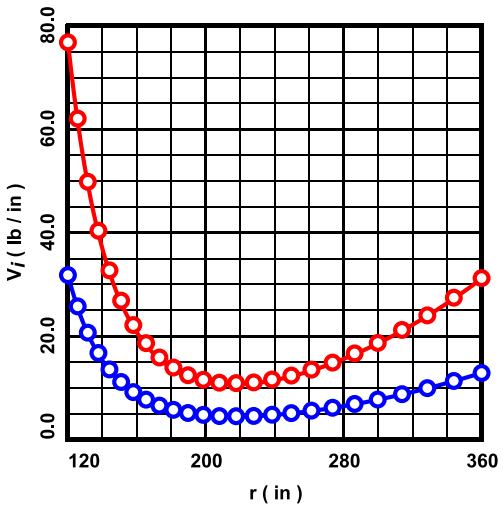

Figure 37. Shear components V_x (red) and V_y (blue) at $\theta = \pi/8$.

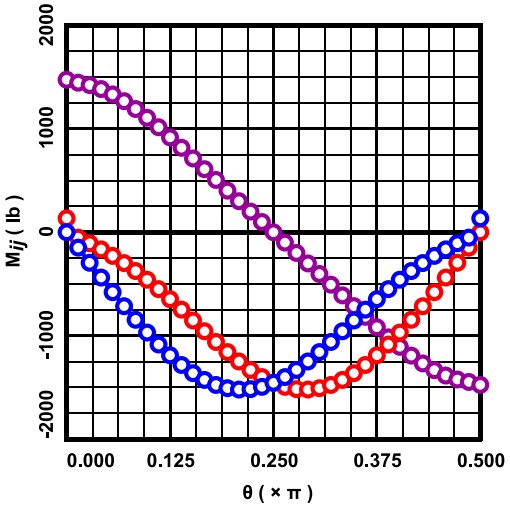

Figure 38. Moment components M_{xy} (red), M_{yx} (blue) and M_{xx} (purple) at $r = 238.442$ in.

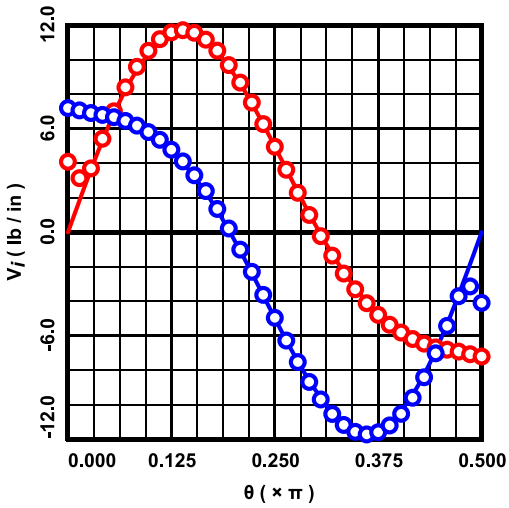

Figure 39. Shear components V_x (red) and V_y (blue) at $r = 238.442$ in.

Figure 38, at above left, gives the numerical results for the moment tensor M_{ij} along the circumferential ring of grid points located at $r = 238.442$ in. Here the behavior of the numerical solution is very similar to that at $r = b$ in Fig. 32. In Fig. 39, at above right, is shown the results along the same ring of grid points for the shear vector V_i. Again, here the behavior is similar to that at $r = b$ in Fig. 33. It is worth mentioning that, in the exact solution, the shear component V_x at $\theta = 0$ and V_y at $\theta = \pi/2$ are zero, *cf.,* the first of eqns. (3.7). As Fig. 39 shows, though, in the numerical solution these values are not zero, but are relatively small, *i.e.,* ~ 4 lb/in.

Finally, the numerically calculated values of the corner forces at the lower right and upper left corners of the domain are, respectively, -3949.36 lb and 3949.34 lb. The exact values of the corner forces are ∓ 3935.94 lb, which amounts to 0.34% relative error.

Overall, except for some errors in the numerically calculated stress resultants at the boundaries, *cf.,* Figs. 31, 32, 33, 38 and 39, for this problem, the cell method is quite accurate and reliable.

8. Closing Remarks

While the author is not aware of anything like the cell method, he thought he would try it out due to its simple and easy to understand idea, *viz.,* just evaluate the governing partial differential equations at the computational grid points. In fact, the cell method is of comparable (if not better) accuracy to both the finite element method and the boundary element method. What is quite astounding, though, is that acceptably accurate solutions to a fourth-order partial differential equation can be obtained by using only quadratic interpolations. Also, the cell method requires that no numerical integrations be performed, unlike in the finite element and boundary element methods. Another point of interest is that, in the finite element method, a C_1 finite element must be used (*e.g.,* the standard fifth-order C_1 triangle element), while in the cell method, any notion of C_1 continuity does not even arise.